CHEMISTRY OF MATERIALS

ARTICLE

pubs.acs.org/cm

Mixed Grotthuss and Vehicle Transport Mechanism in Proton Conducting Polymers from Ab initio Molecular Dynamics Simulations

Guillermo A. Ludueña,[†] Thomas D. Kühne,[‡] and Daniel Sebastiani*[,†,§]

[†]Max-Planck-Institut für Polymerforschung, Ackermannweg 10, 55128 Mainz, Germany

[‡]Institute of Physical Chemistry and Center of Computational Sciences, Johannes Gutenberg University Mainz, Staudinger Weg 9, 55128 Mainz, Germany

[§]Dahlem Center for Complex Quantum Systems, Physics Department, Freie Universität Berlin, Arnimallee 14, 14195 Berlin, Germany

ABSTRACT: We elucidate the microscopic mechanism of long-range proton conduction in poly[vinyl phosphonic acid] (PVPA), a highly promising proton conducting polymer. Using a steered ab initio molecular dynamics approach, we characterize the charge transport functionality of acid groups interacting with nonbulk water molecules intercalated in the polymer. Our results show that in PVPA, unlike in Nafion, water has a local vehicle/carrier function for excess protons. This function must however be combined with the Grotthuss-type conduction mechanism that is supplied by the acid groups in order to yield long-range charge transport. As an additional aspect, we find that contrary to common intuition, systems with disordered/amorphous morphology leave a considerably more pronounced functionality than well-ordered crystalline systems.

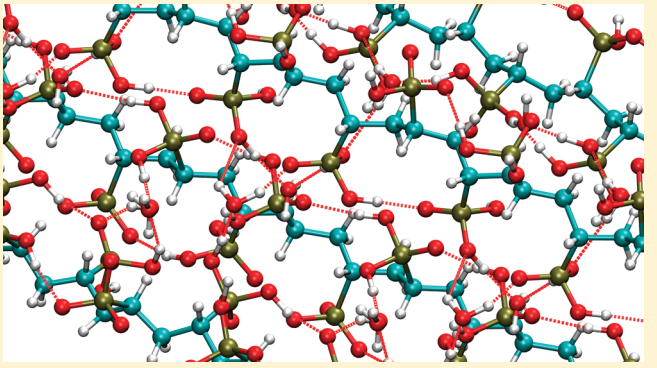

KEYWORDS: ionic conductors, microstructure, theory and modeling

INTRODUCTION

One of the central functional elements of a fuel cell is the ion exchange membrane, which allows only specific ions to migrate to the other electrode while blocking all other particles. Specifically, in the case of a proton exchange membrane fuel cell (PEMFC), an ideal polymer film would be permeable exclusively for protons.

One such polymer based on sulfonic acid end groups is Nafion, whose functionality relies on percolating water channels. Locally, these channels behave similar to bulk water; consequently, they exhibit the same excellent proton conduction observed in homogeneous liquid water. Nafion and related derivatives has been investigated in depth both experimentally[1−6] and computationally.[7−11] The conduction relies on the Grotthuss mechanism,[12] in which proton jumps between water molecules are followed by a local molecular rearrangement. This rearrangement (most often a rotation), in turn, allows the next jump. As an alternative to this Grotthus mechanism, an excess proton can travel on top of a host molecule through the solvent ("vehicle mechanism"). While both transport principles have been extensively studied, there is still an ongoing discussion regarding the nature of the underlying atomistic processes, even in relatively simple and uniform systems like liquid water.[13−17] The corresponding transport processes in more complex environments can be expected to be even more involved than those in homogeneous liquid water.

In the specific field of fuel-cell membrane proton conductors, aqueous proton transport is very common but has an important drawback. To reduce the amount of catalyst that is needed for the dissociation of oxygen molecules at the fuel cell cathode, it is desirable to increase the working temperature of the cell. Naturally, the boiling point of liquid water limits all attempts to push this operating temperature beyond 100 °C, because the proton conducting membrane would fall dry, and proton conduction would come to a halt. Hence, there is a quest for finding high-temperature proton conductors[18] that has brought up polymerized vinyl phosphonic acid (PVPA, see Figure 1). At present, it is believed that this material can be chemically optimized such as to allow for quasi-water-free proton conduction, and thus permitting operating temperatures above 100 °C.[19−25] Preliminary experimental and theoretical studies indicate that in this class of materials, the conduction does not require any bulk water channels, although a certain amount of residual water seems to be necessary to support sustained proton conduction.[26,27] This residual water has properties that differ from conventional bulk water; in particular, it remains inside the polymer at temperatures well beyond the usual boiling point.[28] Hence, the atomistic transport mechanism must differ from the common ideas; at present, there is no clear picture of what is happening on such local scales. The experimentally observed proton conduction[24] persists up to 416 K. Although the actual

Received: September 16, 2010
Revised: January 14, 2011
Published: February 20, 2011

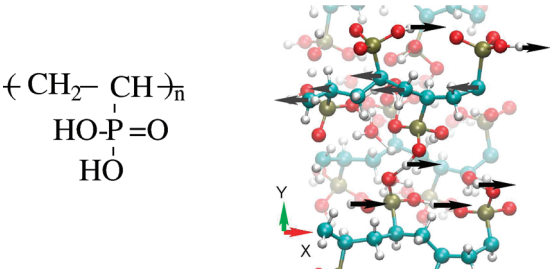

Figure 1. Molecular structure of poly-[vinyl phosphonic acid] (PVPA) and our model system for PVPA. The arrows indicate the external force bias.

conductivity is still below industrial requirements, it is not far from representing a serious alternative to the established materials such as Nafion.

In this work, we present the first attempt to characterize polymerized vinyl phosphonic acid (PVPA) by means of a series of first-principles molecular dynamics (FPMD) simulations. Our specific aim is to simulate long-range proton transport in a realistic model system of PVPA. While molecular phosphonic acid and its derivatives (under both isolated and periodic boundary conditions) have been studied computationally by several groups,[9,16,25,29−32] literature is scarce for fully polymerized phosphonic acid systems.

We study the motion of the H^+ charge carriers resulting from an external driving force that is designed to mimic the proton concentration gradient that is present in an actual fuel cell. We quantify this charge transport by means of a specifically designed collective variable, which is constructed from the ensemble of indistinguishable hydrogen and oxygen atoms in the polymer model. This construction has been inspired by the meta-dynamics scheme.[33−36] This description gives us access to an estimator for the proton conductivity σ, but also allows us to observe the microscopic conduction mechanism of the polymer as a function of environmental conditions such as temperature and water content.

■ COMPUTATIONAL METHODS AND STRUCTURAL MODEL

We have designed a simplified periodic model for the actual PVPA polymer in the condensed phase, illustrated in Figure 1. This model has previously been shown to give a realistic representation of the structure and dynamics of the H-bond network at the atomistic level.[26,27] Four independent linear (syndiotactic) PVPA strands are placed hexagonally with mutual distances of 8 Å under periodic boundary conditions, yielding a unit cell of volume $\Omega = 10.25 \times 13.86 \times 16$ Å^3. Each periodic strand contains four independent phosphonic acid groups, resulting in sixteen PA groups per unit cell. The model is fully periodic in all dimensions and is thus free of surface effects. As in previous studies, the lateral distance between the linear PVPA strands has been extracted from Xray scattering experiments and refined by molecular dynamics simulations.[26,27] This is a fairly simple model for a real polymer, in which many relevant features like tacticity, polymer topology, or density fluctuations are omitted.[37] Nevertheless, the local static and dynamical properties of this particular model could be validated by comparison of experimental NMR chemical shifts and static deuteron NMR lineshapes with the corresponding spectroscopic data obtained from our previous FPMD simulations.[26,27]

Following experimental estimates,[38] our model contains two and eight water molecules intercalated between the polymer chains, which we refer to as "dry" and "wet" PVPA. This concentration corresponds to one water molecule per eight (dry) and per two (wet) phosphonic acid moieties, respectively. The system is further doped with one and two excess protons for the dry and wet models. The corresponding positive ionic charges are compensated by a sufficiently negative homogeneous background charge, to ensure an overall neutrality of the system. The experimental situation in a real fuel cell is that the proton transport is driven by a H^+ concentration gradient, created by the influx of new fuel (H_2 molecules) at the anode and the exothermic reaction $2H^+ + {}^1/_2O_2 + 2e^- \rightarrow H_2O$ at the cathode. Because we cannot model this situation directly, we model the effective force that is generated indirectly by the concentration gradient via Fick's first law by means of a constant force bias $\mathscr{F}$. This effective external force is selectively applied to acidic protons, because these are the particles for which there is a concentration gradient across the fuel cell membrane. It should be noted here that an electric field would not be adequate, because the field in a real fuel cell actually opposes the proton flux and is therefore not the driving force behind the H^+ transport. We believe that our effective force, which is directly applied to the acidic protons, actually represents a considerably better description of the experimental situation (i.e., the H^+ concentration gradient). To have no net force on the entire unit cell, we apply a compensating counterforce to the polymer backbone. A scheme of some of the forward and compensation forces is sketched in Figure 1. The magnitude of this effective force must be large enough to yield a sizable ionic current, but it should not interfere with covalent bonding within the system. An MD run with $\mathscr{F} \sim 200$ pN led to the breaking of a P−O bond, so that we restricted further simulations to forces below 100 pN; specifically, we used $\mathscr{F}$ =30 pN and $\mathscr{F}$ =3 pN. The strength of this force can be compared to the expected value of the effective drag force from the H^+ concentration gradient in a real fuel cell: Assuming equilibrium (no electric current taken from the cell), the absence of a net proton diffusion can be viewed as an equilibrium between the forces from dragging and from the electric potential of the cell. With typical values for cell potential and membrane thickness of 0.7 V and 10 μm, this leads to a force of 0.1 pN. Thus, our forces are about 1−2 orders of magnitude larger than what we have to apply in our molecular dynamics simulations. The need for external driving forces higher than those observed in reality is a typical phenomenon in atomistic simulations. It basically reflects the finite statistical convergence (finite system size, finite simulation time) available to calculations at the highest level of structural detail.

A similar problem exists for the characterization of the atomic dynamics in terms of effective charge transport. On the first-principles level, all protons are treated on an equal footing; it is not possible to distinguish between phosphonic acid protons, "neutral" water protons, and excess protons, because many protons jump between molecules during the FPMD simulations. Therefore, a specific variable has to be created, in order to consolidate the high-dimensional set of coordinate vectors from the FPMD trajectory into a scalar quantity that can be monitored easily, and that represents the effective H^+ charge transport during the simulation.

To this purpose, we have defined a collective variable $\mathscr{Q}$ that measures the position of a fictitious cumulative ionic charge as a function of the translational motion of the protons and other atoms in our simulations. It is given via the atomic coordinates $\mathbf{R}_H$, $\mathbf{R}_O$, and $\mathbf{R}_P$ as

$$\mathscr{Q} := \sum_{H_{ac}} \mathbf{R}_H + w_O \sum_{O} \mathbf{R}_O + w_P \sum_{P} \mathbf{R}_P \qquad (1)$$

with oxygen and phosphorus weighting coefficients $w_O = -2$ and $w_P = N_O - N_H/N_P$ (where N_X is the number of atoms of species X). This choice of the weighting coefficients ensures that the translational motion of neutral water molecules and neutral PA groups is automatically eliminated. By construction, the motion of the polymer backbone does not contribute to the evolution of $\mathscr{Q}$.

Table 1. Left to Right: Decay Rate τ_H^{-1} of the Hydrogen Bond Network Autocorrelation Function, Normalized Ratio p_{H_2O} of Proton Jumps Involving a Water Molecule, Ion Concentration Ratio $[PO_3H_3^+]/[H_3O^+]$, Conductivity σ Obtained from the Average Slope of $\mathcal{Q}$, and Peak Value $P^{max}_{||\Delta\tilde{Q}||}$ at Which the Probability of a Jump Is Maximal (i.e., optimal O−O distance for a H jump)

	wet					dry				
T (K)	$1/\tau_H$ (1/ps)	p_{H_2O} (%)	$[H_3O^+]/[PO_3H_3^+]$	σ (S/cm)	$P^{max}_{\|\Delta\tilde{Q}\|}$	$1/\tau_H$ (1/ps)	p_{H_2O} (%)	$[H_3O^+]/[PO_3H_3^+]$	σ (S/cm)	$P^{max}_{\|\Delta\tilde{Q}\|}$
100	0.0310	95.7	0.680	>0.0001	2.425	0.0525	86.2	0.651	>0.0001	2.403
300	0.0320	26.5	0.011	0.0016	2.415	0.2721	24.8	0.178	0.0073	2.444
400	0.2379	42.7	0.341	0.1100	2.403	0.1490	73.4	0.259	0.0049	2.424
500	0.2888	48.5	0.182	0.5922	2.410	0.2516	7.1	0.014	0.0024	2.419
600	0.2178	47.9	0.180	0.0913	2.416	0.5266	56.6	0.553	0.0738	2.418

The effective ionic current density $\mathcal{J}$ can be obtained as the time derivative of this newly defined collective variable via $\mathcal{J} = e\dot{\mathcal{Q}}(t)/\Omega$. This in turn enables the conversion of $\mathcal{Q}(t)$ into a proton conductivity σ. For this purpose, we have to assume that the effective force $\mathcal{F}$ is created by a (fictitious) electric field $\mathcal{E} = \mathcal{F}/e$. Such a field would act only on the excess charge(s), i.e. our excess protons, whose effective position is described by our collective variable $\mathcal{Q}(t)$ in the model. Using the usual linear relationship between electric field and induced current density, we obtain the following expression for the conductivity:

$$\sigma = \frac{\mathcal{J}}{\mathcal{E}} \times \frac{c_+^{exp}}{c_+^{calc}} = \frac{e^2\dot{\mathcal{Q}}(t)}{\Omega\mathcal{F}} \times \frac{c_+^{exp}}{c_+^{calc}} \quad (2)$$

The density of excess protons in our PVPA model is higher than the concentration in an actual membrane sample. This has an effect on the computed ionic conductivity according to eq 2. To compare σ with the experimentally measured ionic conductivity, in eq 2 we have to scale $\mathcal{J}/\mathcal{E}$ with the ratio of experimental to computational H^+ concentrations c_+^{exp}/c_+^{calc}. As these concentrations reflect the amount of dissociated PAs, the experimentally expected value can be obtained from the equilibrium constant

$$K_a^{\ominus} = \frac{[H^+][HPO_3^-]}{[H_2O][H_2PO_3]} \quad (3)$$

and the charge neutrality condition, if water dissociation is neglected

$$\gamma := \frac{c_+^{exp}}{c_{H_2PO_3}^{exp}} = \sqrt{K_a^{\ominus}\frac{[H_2O]}{[H_2PO_3] + [HPO_3^-]}}. \quad (4)$$

Using the numerical value[39] of phosphoric acid (H_3PO_4) of $K^{\ominus}_{PVPA} = 1.38 \times 10^{-4}$ and an approximate experimental water/acid concentration ratio of $[H_2O]/([H_2PO_3]+[HPO_3^-]) \approx 0.2$,[38] the expected dissociation ratio is $\gamma \approx 5 \times 10^{-3}$. On average, this corresponds to one excess proton per 200 PA groups, whereas our computational model contains a 25 times higher charge carrier concentration in the wet PVPA and 12.5 times higher in the dry PVPA.

Thus, our computed conductivity has to be rescaled in eq 2 by $c_+^{exp}/c_+^{calc} = 1/25 = 0.04$ and $c_+^{exp}/c_+^{calc} = 1/12.5 = 0.02$ respectively for the wet and dry systems at $T = 300$ K. For other temperatures, the factors are adjusted with the law $K_a(T) = \exp[-\Delta G/k_BT] = \exp[\ln(K_a^{300K}) - 300\ K/T]$.

The actual FPMD simulations were carried out in the framework of Kohn−Sham density functional theory,[40,41] using the novel accelerated Car−Parrinello-like molecular dynamics method of Kühne et al.,[42−44] within the CP2K package.[45,46] We used a polarized triple-ζ basis set and a density cutoff of 280 Ry, as well as norm-conserving pseudopotentials[47] and the BLYP[48,49] xc-functional.

RESULTS AND DISCUSSION

Throughout the FPMD simulations, proton jumps do not occur at a constant rate, but rather in events of many coordinated jumps, followed by long periods without relevant activity. Therefore, we have developed specific quantities to describe the behavior of the simulation runs numerically. The structure of the hydrogen bond network is characterized by an N-dimensional vector $\mathbf{H}(t) = (H_k(t))$ where N is the number of acidic protons. Each element $H_k(t)$ of this vector is an integer that represents the atom index of the hydrogen bonding partner of the specific proton k. Numerically, $H_k(t) = j$ if proton k is hydrogen-bonded to oxygen j at time t. In the rare cases where a proton is not H-bonded to any oxygen, $H_k(t)$ is set to zero. Hence, this vector contains all information about the state of the H-bonding network of the entire PVPA simulation box at time t. We further define the H-bond correlation function $\eta(t)$ via

$$\eta(t) = \langle \sum_k \tilde{\delta}_{H_k(t),H_k(0)} \rangle \quad (5)$$

where $\tilde{\delta}_{H_k(t),H_k(0)} = 1$ if $H_k(t)=H_k(0) \neq 0$, and $\tilde{\delta}_{H_k(t),H_k(0)} = 0$ otherwise. This function $\eta(t)$ initially equals the number of H-bonded atoms, i.e., $\eta(0) = N$. In the course of the FPMD simulation, H-bonds break, which leads to a decrease of $\eta(0)$ by one for each broken H-bond. If a H-bond is re-established with the same oxygen as H-bond acceptor, $\eta(t)$ increases by one; in turn, if a H-bond is established with a new acceptor oxygen, the correlation function does not change. Hence, the decay of this function expresses how much of the original H-bonding network (i.e., at time $t = 0$) is lost during the FPMD simulation. In other words, this function counts how many hydrogen bonds have changed after a time t, thus characterizing the dynamics in the hydrogen bonding network. The H-bonding criterion is simply distance-based, i.e., an H-bond is assumed at short distances $r_{OH} < 1.6$ Å[50,51] For our purposes, this relatively simple definition is sufficient, as we only look at a statistical ensemble average of hydrogen bonds.

The function $\eta(t)$ is not sensitive to back-and-forth jumps of protons between two oxygens, in particular when compared to the simple number of proton hopping events. Such oscillatory forth-and-back jumps occur very frequently in our MD simulations but are not relevant for sustained proton conduction. The H-bond dynamics is characterized by a relaxation time via $\tau_H^{-1} = \dot{\eta}(t)/\eta(t)$, which quantifies the effective proton hopping rate in units of jumps per time. $\dot{\eta}(t)$ is computed via finite differences with $\Delta t = 0.1$ ps.

The decay rates τ_H^{-1} for our simulations at $\mathcal{F} = 30$ pN are given in table 1. Except in the 300 K simulation of the wet system, τ_H^{-1} is around one jump per picosecond. Surprisingly, the wet and

dx.doi.org/10.1021/cm102674u |Chem. Mater. 2011, 23, 1424–1429

dry setups yield similar rates for most temperatures. This very mild temperature dependence indicates that the energetic jump barrier is not the rate-limiting quantity for conduction. In fact, it is rather the geometric arrangement of the donor/acceptor oxygens that determines whether a successful jump occurs. In our run at T = 300 K, the configuration of the system remained essentially static for most of the simulation time. This occurs because the system is found in a local minimum within the space of possible configurations, thus blocking the proton transfer events. Analysis of the microstructure shows that the excess protons are not able to reach the water, thus hindering its functionality as a vehicle carrier. This is also reflected in the unusually low values of the conductivity σ and the concentration ratio $[H_3O^+]/[PO_3H_3^+]$ which appear correlated to τ_H^{-1}. A similar situation is observed in the dry simulation at 500 K, where the missing participation of water carriers leads to the absence of charge transport percolation.

We have further analyzed to which degree the jumps of the excess protons occur between two PA grouped and between a PA group and a water molecule. This data is shown in table 1 as the relative rate p_{H_2O} of jumps to or from a water molecule. The values are around 40−50% in the wet system at all temperatures, whereas no universal value can be given for the dry system. The concentration of hydronium ions relative to charged phosphonic groups is about 20% in the wet system and generally below 50% in the dry at high temperatures. This indicates that the excess protons jump with the same probability to a water or to a phosphonic group, but H_3O^+ ions are formed only briefly. Thus, water molecules have mainly just a bridge functionality for the hopping between phosphonic groups. The apparently inverse $[H_3O^+]/[PO_3H_3^+]$ ratio is due to the much higher concentration of acid groups with respect to water.[52]

All components of the conduction variable ($\mathcal{Q}_x, \mathcal{Q}_y, \mathcal{Q}_z$) show uncorrelated oscillations of amplitude ∼10 Å. These oscillations correspond to local intra- and interchain hopping of the protons, as well as the regular motion of the vibrational modes of the polymer and the water molecules. Both types of motion are not relevant for sustained long-range charge transport, because the protons will simply iterate periodically between the same groups.

The mechanism of interest is characterized by the evolution of the component $\mathcal{Q}_x$ parallel to the external driving force on the time scale of picoseconds. This data is shown in Figure 2 for three temperatures. The straight lines are linear regressions of the actual data. The starting values $\mathcal{Q}(t = 0)$ have been shifted such that the regression has a zero intercept at t = 0. The top plot shows that for $\mathcal{F}$ = 3 pN, there is virtually no change in $\mathcal{Q}_x$ above the noise level during the trajectory of 25 ps duration, neither for the dry (gray line) nor for the wet (black line) PVPA model. Increasing the external driving force 10-fold (to $\mathcal{F}$ = 30 pN, shown in the middle and bottom plots of Figure 2) leads to a significant trend of $\mathcal{Q}_x$ for the wet model at T = 400 K (center graph) and an even stronger trend at T = 500 K (bottom graph). The dry setup, in turn, exhibits a certain drift in $\mathcal{Q}_x$, but with a magnitude that is smaller than the statistical noise (and considerably smaller than the drift in the humidified polymer).

In combination with the proton jump rates (Table 1), this shows again that the long-range transport of excess protons is hindered in the dry environment despite the numerous successful proton jump events. Closer inspection of our trajectories reveals that interruptions of the percolating hydrogen bond network are responsible for the absence of persistent conduction.

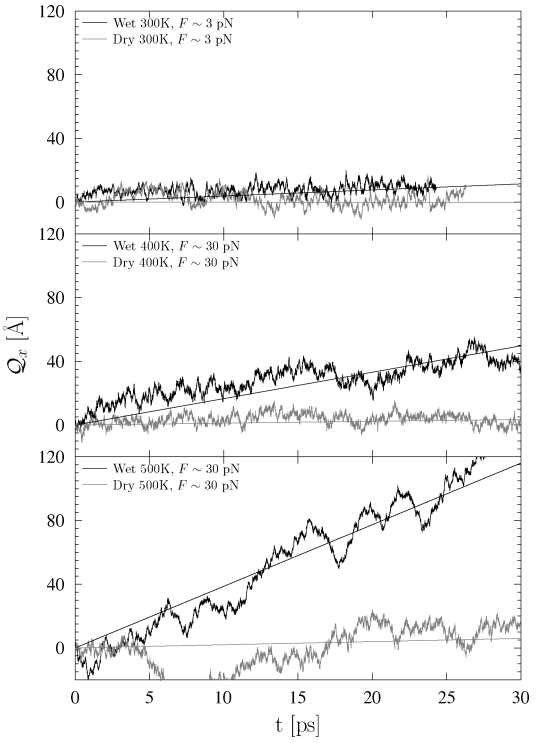

Figure 2. Evolution of the component of $\mathcal{Q}_x$ in the axis of the applied force for dry and wet PVPA, under different temperatures.

The numerical values of the ionic conductivities derived via eqs 1 and 2 are also summarized in 1. The wet conductivity strongly increases with temperature, with the exception of T = 600 K. This might be related to the conductivity plateau that is experimentally observed for T > 400 K.[53] The material itself also degrades above 500 K.[38,54]

We can analyze the system further by looking at the evolution of a modified version $\tilde{Q}$ of the conduction variable $\mathcal{Q}$. In comparison to $\mathcal{Q}$, all hydrogens are projected onto the position of the nearest oxygen. This definition ensures $\tilde{Q}(t) \approx \mathcal{Q}(t)$ for large times t, but the time evolution of the new variable $\tilde{Q}$ is now stepwise. For this new variable, the magnitude of the change $\Delta\tilde{Q}$ at a given moment (when a proton jump from one oxygen to another is observed) equals the oxygen−oxygen distance at the moment of this jump. Thus, the distribution of $\tilde{Q}$ describes the probability of a given oxygen−oxygen distance at the moment of a proton jump. The histogram of steps in $\tilde{Q}$ is given in Figure 3. This distribution $\mathcal{P}(||\Delta\tilde{Q}||)$ quantifies the probability of a jump for a given O−O distance. The narrow peak at $||\Delta\tilde{Q}|| \sim 2.4$ Å is universal for both dry and wet systems at all temperatures. This in turn illustrates that the dynamics in both systems is governed by precisely the same mechanism.

■ CONCLUSION

In summary, we have provided an atomistic picture of the proton conduction mechanism of PVPA. The outcome of our study shows that residual water molecules are required as short-distance vehicles for sustained proton conduction, in agreement with experimental observations. We find that local proton hopping between adjacent acids occurs very frequently, but does not contribute to sustained net charge transport. The Grotthuss-style hopping mechanism must be supported by short-distance

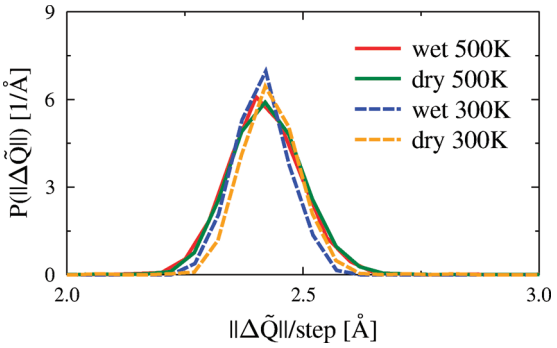

Figure 3. Distribution of $\Delta\tilde{Q}$ between successive MD timesteps (0.5 fs) for the wet and dry systems at 300 and 500 K. This function $P(\|\Delta\tilde{Q}\|)$ represents the distribution of oxygen−oxygen distances at the moment of an H^+ jump event.

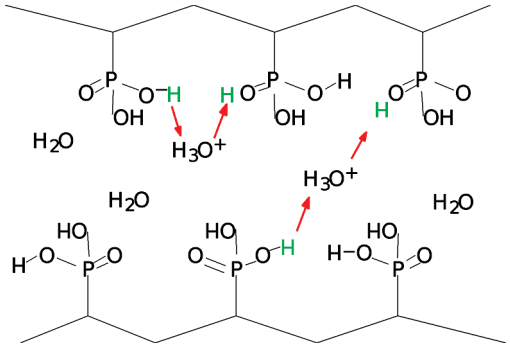

Figure 4. Scheme of the suggested mechanism, where a Grotthuss-style hopping mechanism is supported by short-distance transport of hydronium ions to neighboring acids. We call this a carrier-mediated Grotthuss mechanism.

transport of hydronium ions to neighboring acids. On the other hand, the hydrogen-bond network is dense enough to inhibit large-distance vehicular transport of hydroniums. Thus, the main role of water is to bridge the H-bond percolation path, complementing Grotthuss proton hopping between phosphonic acid groups. We call this a carrier-mediated Grotthuss mechanism (see Figure 4).

Our microscopic picture of a water-mediated Grotthus transport mechanism feeds hope that the functionality of intercalated water molecules as intermediary for short-range proton hopping could be taken by other functional groups, thus obviating the need of water in the material. It certainly still represents a synthetic challenge to establish flexibly anchored groups with this functionality. However, such a material would enable sustained proton conduction well beyond the boiling point of water.

AUTHOR INFORMATION

Corresponding Author

*E-mail: daniel.sebastiani@fu-berlin.de.

ACKNOWLEDGMENT

This work was supported by DFG Grants Se 1008/5-1 and Se 1008/6-1. We thank A. Kaltbeitzel, L. Jiménez García, Y. J. Lee, and H. W. Spiess for valuable discussions.

REFERENCES

(1) Krivobokov, I. M.; Gribov, E. N.; Okunev, A. G.; Spoto, G.; Parmon, V. N. *Solid State Ionics* **2010**, *180*, 1694–1701.
(2) Schuster, M. F. H.; Meyer, W. H.; Schuster, M.; Kreuer, K. D. *Chem. Mater.* **2004**, *16*, 329–337.
(3) Sharif, S.; Denisov, G.; Toney, M.; Limbach, H. *J. Am. Chem. Soc.* **2006**, *128*, 3375–3387.
(4) Jiménez-García, L.; Kaltbeitzel, A.; Pisula, W.; Gutmann, J. S.; Klapper, M.; Müllen, K. *Angew. Chem., Int. Ed.* **2009**, *48*, 9951–9953.
(5) Schmidt-Rohr, K.; Chen, Q. *Nat. Mater.* **2008**, *7*, 75–83.
(6) Kalapos, T.; Decker, B.; Every, H.; Ghassemi, H.; Zawodzinski., T. *J. Power Sources* **2007**, *172*, 14–19ACS San Francisco 2006, Fuel and Cell Symposium. American Chemical Society National Meeting. San Francisco, CA Sept 10−14 2006..
(7) Boero, M.; Ikeshoji, T.; Terakura, K. *ChemPhysChem* **2005**, *6*, 1775–1779..
(8) Paddison, S. J.; Paul, R. *Phys. Chem. Chem. Phys.* **2002**, *4*, 1158–1163.
(9) Markovitch, O.; Chen, H.; Izvekov, S.; Paesani, F.; Voth, G. A.; Agmon, N. *J. Phys. Chem. B* **2008**, *112*, 9456–9466.
(10) Tuckerman, M.; Laasonen, K.; Sprik, M.; Parrinello, M. *J. Chem. Phys.* **1995**, *103*, 150–161.
(11) Hayes, R. L.; Paddison, S. J.; Tuckerman, M. E. *J. Phys. Chem. B* **2009**, *113*, 16574–16589.
(12) de Grotthuss, C. J. T. *Ann. Chim.* **1806**, *58*, 54–73.
(13) Paesani, F.; Voth, G. A. *J. Phys. Chem. B* **2009**, *113*, 5702–5719.
(14) Chen, H.; Voth, G. A.; Agmon, N. *J. Phys. Chem. B* **2010**, *114*, 333–339.
(15) Cao, Z.; Peng, Y.; Yan, T.; Li, S.; Li, A.; Voth, G. A. *J. Am. Chem. Soc.* **2010**, *132*, 11395–11397.
(16) Habenicht, B. F.; Paddison, S. J.; Tuckerman, M. E. *Phys. Chem. Chem. Phys.* **2010**, *12*, 8728–8732.
(17) Wang, C.; Paddison, S. J. *Phys. Chem. Chem. Phys.* **2010**, *12*, 970–981.
(18) Paddison, S. *Ann. Rev. Mater. Res.* **2003**, *33*, 289–319.
(19) Goktepe, F.; Celik, S. U.; Bozkurt, A. *J. Non-Cryst. Solids* **2008**, *354*, 3637–3642.
(20) Aslan, A.; Celik, S. U.; Bozkurt, A. *Solid State Ion.* **2009**, *180*, 1240–1245.
(21) Perrin, R.; Elomaa, M.; Jannasch, P. *Macromolecules* **2009**, *42*, 5146–5154.
(22) Aslan, A.; Bozkurt, A. *J. Power Sources* **2009**, *191*, 442–447.
(23) Pan, F.; Jia, H.; Jiang, Z.; Zheng, X. *J. Membr. Sci.* **2008**, *325*, 727–734.
(24) Jiang, F.; Kaltbeitzel, A.; Fassbender, B.; Brunklaus, G.; Pu, H.; Meyer, W. H.; Spiess, H. W.; Wegner, G. *Macromol. Chem. Phys.* **2008**, *209*, 2494–2503.
(25) Vilciauskas, L.; Paddison, S.; Kreuer, K. *J. Phys. Chem. A* **2009**, *113*, 9193–9201.
(26) Lee, Y. J.; Bingöl, B.; Murakhtina, T.; Sebastiani, D.; Meyer, W.; Wegner, G.; Spiess, H. *J. Phys. Chem. B* **2007**, *111*, 9711–9721.
(27) Lee, Y. J.; Murakhtina, T.; Sebastiani, D.; Spiess, H. *J. Am. Chem. Soc.* **2007**, *129*, 12406–12407.
(28) Steininger, H.; Schuster, M.; Kreuer, K. D.; Kaltbeitzel, A.; Bingöl, B.; Meyer, W. H.; Schauff, S.; Brunklaus, G.; Maier, J.; Spiess, H. W. *Phys. Chem. Chem. Phys.* **2007**, *9*, 1764–1741.
(29) Habenicht, B. F.; Paddison, S. J.; Tuckerman, M. E. *J. Mater. Chem.* **2010**, *20*, 6342–6351.
(30) Paddison, S. J.; Elliott, J. A. *Solid State Ionics* **2006**, *177*, 2385–2390.
(31) Paddison, S. J.; Kreuer, K.-D.; Maier, J. *Phys. Chem. Chem. Phys.* **2006**, *8*, 4530–4542.
(32) Paddison, S. J.; Elliott, J. A. *Phys. Chem. Chem. Phys.* **2006**, *8*, 2193–2203.
(33) Laio, A.; Parrinello, M. *Proc. Natl. Acad. Sci. U.S.A.* **2002**, *99*, 12562–12566.

(34) Iannuzzi, M.; Laio, A.; Parrinello, M. *Phys. Rev. Lett.* **2003**, *90*, 238302.
(35) Iannuzzi, M.; Parrinello, M. *Phys. Rev. Lett.* **2004**, *93*, 025901.
(36) Iannuzzi, M. *J. Chem. Phys.* **2006**, *124*, 204710.
(37) Binder, K. *Monte Carlo and Molecular Dynamics Simulations in Polymer Science*; Oxford University Press: Oxford, U.K., 1995.
(38) Kaltbeitzel, A.; Schauff, S.; Steininger, H.; Bingöl, B.; Brunklaus, G.; Meyer, W. H.; Spiess, H. W. *Solid State Ionics* **2007**, *178*, 469–474.
(39) Franz, R. G. *AAPS Pharmsci.* **2001**, *3*, 10.
(40) Kohn, W.; Sham, L. J. *Phys. Rev.* **1965**, *140*, A1133.
(41) Jones, R. O.; Gunnarsson, O. *Rev. Mod. Phys.* **1989**, *61*, 689–746.
(42) Kühne, T. D.; Krack, M.; Mohamed, F.; Parrinello, M. *Phys. Rev. Lett.* **2007**, *6*, 066401.
(43) Kühne, T. D.; Krack, M.; Parrinello, M. *J. Chem. Theory Comput.* **2009**, *5*, 235–241.
(44) Cucinotta, C. S.; Miceli, G.; Raiteri, P.; Krack, M.; Kuehne, T. D.; Bernasconi, M.; Parrinello, M. *Phys. Rev. Lett.* **2009**, *103*, 125901.
(45) Lippert, G.; Hutter, J.; Parrinello, M. *Mol. Phys.* **1997**, *92*, 477–487.
(46) Vondele, J. V.; Krack, M.; Mohamed, F.; Parrinello, M.; Chassaing, T.; Hutter, J. *Comput. Phys. Commun.* **2005**, *167*, 103–128.
(47) Goedecker, S.; Teter, M.; Hutter, J. *Phys. Rev. B* 1996, *54*, 1703.
(48) Becke, A. D. *Phys. Rev. A* **1988**, *38*, 3098.
(49) Lee, C.; Yang, W.; Parr, R. G. *Phys. Rev. B* **1988**, *37*, 785–789.
(50) Kumar, R.; Schmidt, J. R.; Skinner, J. L. *jcp* **2007**, *126*, 204107.
(51) Kumar, R.; Schmidt, J. R.; Skinner, J. L. *J. Chem. Phys.* **2007**, *126*, 204107.
(52) Munson, R. A. *J. Phys. Chem.* **1964**, *68*, 3374–3377.
(53) Kaltbeitzel, A. private communication, 2009.
(54) Jiang, D. D.; Yao, Q.; McKinney, M. A.; Wilkie, C. A. *Polym. Degrad. Stab.* **1999**, *63*, 423–434.